Preclinical Evaluation of a Radiotheranostic Single-Domain Antibody Against Fibroblast Activation Protein α

Yana Dekempeneer[1], Sam Massa[1], Francis Santens[1], Laurent Navarro[1], Marion Berdal[1], Melissa Miranda Lucero[1], Ana Rita Pombo Antunes[1], Tony Lahoutte[1–3], Jo A. Van Ginderachter[4,5], Nick Devoogdt*[1,2], and Matthias D'Huyvetter*[1,2]

[1]*Precirix NV/SA, Brussels, Belgium;* [2]*Department of Medical Imaging, In Vivo Cellular and Molecular Imaging Laboratory, Vrije Universiteit Brussel, Brussels, Belgium;* [3]*Department of Nuclear Medicine, UZ Brussel, Brussels, Belgium;* [4]*Laboratory of Cellular and Molecular Immunology, Vrije Universiteit Brussel, Brussels, Belgium; and* [5]*Myeloid Cell Immunology Lab, VIB Center for Inflammation Research, Brussels, Belgium*

Fibroblast activation protein α (FAP) is highly expressed on cancer-associated fibroblasts of epithelial-derived cancers. Breast, colon, and pancreatic tumors often show strong desmoplastic reactions, which result in a dominant presence of stromal cells. FAP has gained interest as a target for molecular imaging and targeted therapies. Single-domain antibodies (sdAbs) are the smallest antibody-derived fragments with beneficial pharmacokinetic properties for molecular imaging and targeted therapy. **Methods:** We describe the generation, selection, and characterization of a sdAb against FAP. In mice, we assessed its imaging and therapeutic potential after radiolabeling with tracer-dose ^{131}I and ^{68}Ga for SPECT and PET imaging, respectively, and with ^{131}I and ^{225}Ac for targeted radionuclide therapy. **Results:** The lead sdAb, 4AH29, exhibiting picomolar affinity for a distinct FAP epitope, recognized both purified and membrane-bound FAP protein. Radiolabeled versions, including [^{68}Ga]Ga-DOTA-4AH29, [^{225}Ac]Ac-DOTA-4AH29, and [^{131}I]I-guanidinomethyl iodobenzoate (GMIB)-4AH29, displayed radiochemical purities exceeding 95% and effectively bound to recombinant human FAP protein and FAP-positive GM05389 human fibroblasts. These radiolabeled compounds exhibited rapid and specific accumulation in human FAP–positive U87-MG glioblastoma tumors, with low but specific uptake in lymph nodes, uterus, bone, and skin (~2–3 percentage injected activity per gram of tissue [%IA/g]). Kidney clearance of unbound [^{131}I]I-GMIB-4AH29 was fast (<1 %IA/g after 24 h), whereas [^{225}Ac]Ac-DOTA-4AH29 exhibited slower clearance (8.07 ± 1.39 %IA/g after 24 h and 2.47 ± 0.18 %IA/g after 96 h). Mice treated with [^{225}Ac]Ac-DOTA-4AH29 and [^{131}I]I-GMIB-4AH29 demonstrated prolonged survival compared with those receiving vehicle solution. **Conclusion:** [^{68}Ga]Ga-DOTA-4AH29 and [^{131}I]I-GMIB-4AH29 enable precise FAP-positive tumor detection in mice. Therapeutic [^{225}Ac]Ac-DOTA-4AH29 and [^{131}I]I-GMIB-4AH29 exhibit strong and sustained tumor targeting, resulting in dose-dependent therapeutic effects in FAP-positive tumor-bearing mice, albeit with kidney toxicity observed later for [^{225}Ac]Ac-DOTA-4AH29. This study confirms the potential of radiolabeled sdAb 4AH29 as a radiotheranostic agent for FAP-positive cancers, warranting clinical evaluation.

Key Words: fibroblast activation protein α; single-domain antibodies; radiotheranostics; targeted radionuclide therapy

J Nucl Med 2023; 64:1941–1948
DOI: 10.2967/jnumed.123.266381

Targeted radionuclide therapy (TRT) can be a relevant strategy for systemic malignancies. In TRT, radiolabeled compounds are systemically administered with an aim to deliver cytotoxic radiation to diseased sites (*1*). In doing so, targeting moieties are coupled to α-emitting, β-emitting, or Auger electron–emitting radionuclides. Different types of moieties have been used, of which monoclonal antibodies have been explored abundantly (*2,3*), but their limited tissue penetration and off-target effects have hindered progress. With the introduction of monoclonal antibody fragments, peptides, and small molecules, the field of TRT has undergone a revitalization, highlighted by recent success stories with [^{177}Lu]Lu-DOTATATE and [^{177}Lu]Lu-PSMA-617 (*4,5*). An interesting class of monoclonal antibody fragments comprises single-domain antibodies (sdAbs). High binding affinity and specificity, fast blood clearance, and the ability to homogeneously distribute in target tissues make sdAbs promising targeting moieties for diagnostic imaging and TRT (*6,7*).

Fibroblast activation protein α (FAP) is overexpressed on cancer-associated fibroblasts in various carcinomas, contributing to tumor growth, metastasis, and immunosuppression (*8*). Breast, colon, and pancreatic tumors often show strong desmoplastic reactions, which result in a dominant presence of stromal cells. In particular cases, cancer cells express FAP as well, such as in sarcomas, melanomas, or glioblastomas. FAP targeting is gaining attention for molecular imaging and TRT. Quinoline-based FAP inhibitors (FAPIs) have shown potential in cancer imaging, but their prognostic value remains uncertain. Some FAPI molecules have been labeled with therapeutic radionuclides and evaluated in preclinical and clinical studies, although clinical evidence is limited and shows mixed responses to anti-FAP TRT. Challenges include small patient cohorts, heterogeneity, and optimizing FAPI tumor retention (*9*).

Here we describe the generation, selection, and characterization of a lead sdAb with excellent binding characteristics for FAP. We assessed its PET and SPECT imaging potential, as well as its use for TRT.

Received Jul. 17, 2023; revision accepted Sep. 27, 2023.
For correspondence or reprints, contact Matthias D'Huyvetter (matthias.dhuyvetter@precirix.com).
*Contributed equally to this work.

MATERIALS AND METHODS

The methodologies for sdAb generation (*10,11*), lead compound selection and biochemical characterization, cell culture conditions, radiochemical procedures, radioligand binding studies, and dosimetry calculations can be found in the supplemental materials (supplemental materials are available at http://jnm.snmjournals.org).

Preparation of Radiolabeled sdAbs

For in vitro binding studies and small-animal SPECT/CT imaging in mice, His_6-tagged anti-FAP sdAbs, along with control sdAb R3B23, were radiolabeled with ^{99m}Tc. The radiolabeling involved the incorporation of ^{99m}Tc into the His_6 tag using tricarbonyl chemistry (*10,12*). For small-animal SPECT/CT imaging and TRT, [^{131}I]-guanidinomethyl iodobenzoate (GMIB)-4AH29 and [^{131}I]I-GMIB-R3B23 were obtained at tracer doses and therapeutic levels. This radiolabeling process involved a 2-step procedure using the *N*-succinimidyl guanidinomethyl iodobenzoate (SGMIB) tin precursor to attach ^{131}I to 4AH29 and R3B23. Pure [^{131}I]I-GMIB-4AH29 and [^{131}I]I-GMIB-R3B23 were obtained after purification through size-exclusion chromatography. For small-animal PET/CT imaging and TRT, protein intermediates DOTA-4AH29 and DOTA-R3B23 were prepared for labeling with ^{68}Ga and ^{225}Ac. This process involved incubating DOTA-4AH29 and DOTA-R3B23 with the desired activity of ^{68}Ga and ^{225}Ac at 50°C for 10–30 min, followed by purification using size-exclusion chromatography to obtain [^{68}Ga]Ga-DOTA-4AH29, [^{68}Ga]Ga-DOTA-R3B23, [^{225}Ac]Ac-DOTA-4AH29, and [^{225}Ac]Ac-DOTA-R3B23. Radiochemical purity was assessed via instant thin-layer chromatography.

Animal Models

Female CRL:ν-FoxN1nu mice (Charles River) received subcutaneous neck injections of 2×10^6 U87-MG cells. Tumors were allowed to grow to 100–250 mm^3 for biodistribution and therapy studies. We monitored animal welfare by measuring weights and tumor volumes, applying a humane endpoint of body weight loss of more than 20% or tumor volume of more than 1,500 mm^3. Tumor dimensions were calculated using a digital caliper. Dose-escalation studies were performed on female C57BL/6 mice (Charles River). Ethical approval was granted by Vrije Universiteit Brussel's ethical committee.

Biodistribution of Radiolabeled sdAbs

CRL:ν-FoxN1nu mice with human FAP (hFAP)–positive U87-MG tumors sized 100–250 mm^3 received intravenous injections of ^{99m}Tc- and ^{68}Ga-labeled sdAbs. Imaging was conducted 1 h after tracer administration using small-animal SPECT/CT Vector+/CT (MILabs) or small-animal PET/CT β/X-CUBE (Molecubes) systems. [^{131}I]I-GMIB-R3B23 and [^{131}I]I-GMIB-4AH29 were imaged at various time points using the Vector+/CT system. After imaging, mice were euthanized, and organs and tissues were weighed. Time-dependent biodistributions of [^{131}I]I-GMIB-4AH29 and [^{225}Ac]Ac-DOTA-4AH29 were determined through dissections up to 96 h after injection, and dosimetry calculations were performed as described previously (*13,14*).

Toxicity Assessment of Therapeutic [^{131}I]I-GMIB-4AH29 and [^{225}Ac]Ac-DOTA-4AH29

[^{131}I]I-GMIB-4AH29 and [^{225}Ac]Ac-DOTA-4AH29 were administered to healthy mice in a dose-escalation study, with a 6-mo follow-up period. C57BL/6 mice ($n = 5$) received intravenous injections 6 times over 3 wk, with doses ranging from 37 to 4.63 MBq for [^{131}I]I-GMIB-4AH29 and from 40 to 2.5 kBq for [^{225}Ac]Ac-DOTA-4AH29 (each < 30 μg). Control groups received only vehicle solution. Mice were euthanized on reaching specific endpoints: more than 20% weight loss, body condition scoring, or significant changes in behavior. Organs and tissues were collected, fixed, and examined for signs of toxicity via hematoxylin-and-eosin staining and light microscopy.

Therapeutic Efficacy of [^{131}I]I-GMIB-4AH29 and [^{225}Ac]Ac-DOTA-4AH29

To assess the therapeutic impact of [^{131}I]I-GMIB-4AH29 and [^{225}Ac]Ac-DOTA-4AH29, groups of mice ($n = 10$) with hFAP-positive U87-MG tumors were intravenously treated 6 times over 3 wk with 38.60 ± 0.36 MBq of [^{131}I]I-GMIB-4AH29, 18.73 ± 0.16 MBq of [^{131}I]I-GMIB-4AH29, 20.43 ± 0.48 kBq of [^{225}Ac]Ac-DOTA-4AH29, 5.14 ± 0.14 kBq of [^{225}Ac]Ac-DOTA-4AH29 (each < 30 μg), or vehicle solution. Mice were euthanized on meeting any of these criteria: more than 20% weight loss, body condition scoring, notable behavioral changes, or tumor size of at least 1,500 mm^3.

Statistical Analysis

Kaplan–Meier curves that show the time to reach humane endpoints were statistically analyzed using the log-rank (Mantel–Cox) test. Student *t* testing or 1-way ANOVA were performed for all other results.

RESULTS

Generation and In Vitro and In Vivo Screening of Anti-FAP sdAbs

As described in the supplemental materials, we developed 4 anti-FAP sdAbs, of which 4AH29 is the lead for further clinical development. In an enzyme-linked immunosorbent assay, 4AH29 binds both mouse FAP (mFAP) and hFAP, 4HB139 is cross-reactive but shows weaker binding to mFAP, 2MR158 is an hFAP binder, and 2MS56 is an mFAP binder. A homology plot of the FAP sequence of different species is shown in Supplemental Figure 1. All hFAP binders equally recognize cynomolgus FAP protein. In these assays, no sdAb binds human dipeptidyl peptidase-4, the closest homolog of FAP in humans, showing the specificity of the binding (Supplemental Fig. 1A). Biolayer interferometry measurements confirmed these binding profiles, with the lead compound, 4AH29, having an affinity of 38 pM for hFAP protein (Table 1; Supplemental Fig. 3). Next, we investigated whether the sdAbs influenced enzymatic activity of the FAP protein. In contrast to FAPI-4 and talabostat, which bind to the catalytic pocket of the enzyme and inhibit it, none of the 4 sdAbs influenced the rate of conversion of a fluorogenic substrate (Table 2; Supplemental Fig. 2D). The 4 sdAbs bound to GM05389 human fibroblasts, mFAP- or hFAP-transfected HEK293 cells, and U87-MG cells, all cells that express either mFAP or hFAP, as measured by flow cytometry (Supplemental Figs. 2C, 4, and 5). 4AH29, 4HB139, 2MR158, and 2MS56 were successfully radiolabeled with ^{99m}Tc (Supplemental Table 1).The half-maximal effective concentration (EC_{50}) values of [^{99m}Tc]Tc-4AH29, [^{99m}Tc]Tc-4HB139, [^{99m}Tc]Tc-2MR158, and [^{99m}Tc]Tc-2MS56 were obtained on the same cell lines as described earlier (Supplemental Figs. 2B and 6) and were in line with results obtained through flow cytometry. In vivo, the ^{99m}Tc sdAbs revealed a typical pattern of fast-clearing radiolabeled small proteins, with low levels of radioactivity in all organs and tissues, including blood, and high radioactivity levels in the kidneys (Figs. 1A and 1C; Supplemental Table 2). As expected, the ^{99m}Tc-labeled hFAP-binding sdAbs 4AH29, 4HB139, and 2MR158 showed significantly higher uptake in hFAP-expressing U87-MG

TABLE 1
Kinetic Binding Analysis of sdAbs to Biotinylated hFAP or mFAP Protein

	hFAP			mFAP		
sdAb	k_{on} (1/Ms)	k_{off} (1/s)	K_D (M)	k_{on} (1/Ms)	k_{off} (1/s)	K_D (M)
4AH29	7.0E+05	2.7E−05	37.8E−12	1.9E+06	1.4E−03	742.0E−12
4HB139	4.2E+05	3.1E−05	74.4E−12	3.4E+05	8.2E−03	24.3E−9
2MR158	3.4E+05	5.4E−05	160.0E−12	ND	ND	ND
2MS56	ND	ND	ND	1.1E+06	5.6E−04	512.0E−12

k_{on} = association rate constant; k_{off} = dissociation rate constant; K_D = equilibrium dissociation constant; ND = not determined.
Data are representative of 3 independent experiments.

tumors than did [^{99m}Tc]Tc-2MS56, which binds only mFAP ($P < 0.0001$). Levels in blood and vascularized tissues were slightly elevated for [^{99m}Tc]Tc-4AH29, [^{99m}Tc]Tc-2MS56, and [^{99m}Tc]Tc-4HB139, which bind the mFAP protein. This elevated uptake could potentially be attributed to the presence of circulating FAP protein in mice (but not in humans), as suggested by Keane et al. (*15*). [^{99m}Tc]Tc-2MS56 exhibited higher liver uptake than that of 4HB139, 4AH29, and 2MR158. This might result from its lower melting temperature of 61.5°C, in contrast to the melting temperature of more than 65°C of the others. This could result in more aggregate formation during radiolabeling at 50°C, potentially causing formation of aggregates that are trapped in the liver (*12*).

Conjugation and Radiolabeling of sdAbs

The DOTA–sdAb conjugates were purified via size-exclusion high-performance liquid chromatography and analyzed using liquid chromatography–mass spectrometry, which revealed a mixture of unconjugated sdAb and sdAb conjugated to 1–5 DOTA molecules (Supplemental Fig. 7). The lead sdAb, 4AH29, or the control sdAb, R3B23, was successfully radiolabeled with [^{131}I]I-SGMIB or ^{68}Ga/^{225}Ac after DOTA conjugation, yielding a decay-corrected radiochemical yield of 62.7%–77.8% and radiochemical purity of more than 98.4% (Supplemental Table 1).

Cell Binding and Immunoreactivity

[^{131}I]I-GMIB-4AH29 and [^{225}Ac]Ac-DOTA-4AH29 bound hFAP-positive GM05389 cells with EC_{50} values of 0.6 ± 0.7 and 0.4 ± 0.1 nM, respectively, and exhibited sustained cell-associated activity, retaining more than 80% of the initial bound activity after 24 h. The immunoreactive fractions were 98.3% for [^{131}I]I-GMIB-4AH29 and 83% for [^{225}Ac]Ac-DOTA-4AH29, demonstrating that radiolabeling did not affect binding affinity (Supplemental Fig. 8).

Imaging, Biodistribution, and Dosimetry

Small-animal SPECT/CT and PET/CT imaging, along with ex vivo examinations, demonstrated fast and robust uptake of [^{68}Ga]Ga-DOTA-4AH29 and [^{131}I]I-GMIB-4AH29 in hFAP-positive U87-MG tumors (Figs. 1B and 2A; Supplemental Tables 3 and 4). [^{131}I]I-GMIB-4AH29 exhibited rapid kidney clearance and minimal accumulation in thyroid, liver, heart, and lungs (Fig. 2A).

Long-term biodistribution studies with [^{131}I]I-GMIB-4AH29 and [^{225}Ac]Ac-DOTA-4AH29 up to 96 h after injection in U87-MG tumor–bearing mice facilitated dosimetry calculations. [^{131}I]I-GMIB-4AH29 resulted in substantial tumor retention (15.62 ± 2.49 percentage injected activity per gram of tissue [%IA/g] at 1 h and 5.93 ± 1.00 %IA/g at 72 h) and rapid clearance from kidneys (0.74 ± 0.18% IA/g at 24 h and 0.68 ± 0.21 %IA/g at 72 h; Fig. 2B; Supplemental Table 5). Tumor-to-kidney ratios improved from 0.35 ± 0.03 at 1 h to 10.08 ± 2.69 at 72 h (Fig. 2B). [^{225}Ac]Ac-DOTA-4AH29 revealed a tumor uptake of 4.18 ± 0.16 %IA/g at 1 h and 6.51 ± 0.12 %IA/g at 6 h, with a slower kidney clearance (12.41 ± 1.52 %IA/g at 1 h and 3.68 ± 0.56 %IA/g at 72 h; Fig. 2C; Supplemental Table 6). Tumor-to-kidney ratios

TABLE 2
Influence of Equimolar Concentration of SdAbs and Small-Molecule Inhibitors Talabostat and FAPI-4 on hFAP Enzymatic Activity

hFAP	+	+	+	+	+	+	+	+	+	+	+	+	+	+	+	−
FAPI-4	−	+	−	−	+	−	−	+	−	−	+	−	−	+	−	−
Talabostat	−	−	+	−	−	+	−	−	+	−	−	+	−	−	+	−
4AH29	−	−	−	+	+	+	−	−	−	−	−	−	−	−	−	−
4HB139	−	−	−	−	−	−	+	+	+	−	−	−	−	−	−	−
2MR158	−	−	−	−	−	−	−	−	−	+	+	+	−	−	−	−
2MS56	−	−	−	−	−	−	−	−	−	−	−	−	+	+	+	−
FAP activity	1.5	0.0	0.1	1.4	0.0	0.1	1.4	0.0	0.1	1.4	0.0	0.1	1.1	0.0	0.2	0.0

− = absent; + = present.
Bottom row provides slopes of fluorogenic substrate cleavage curves in function of time, per condition (Supplemental Fig. 2D). One representative of 3 independent experiments is shown.

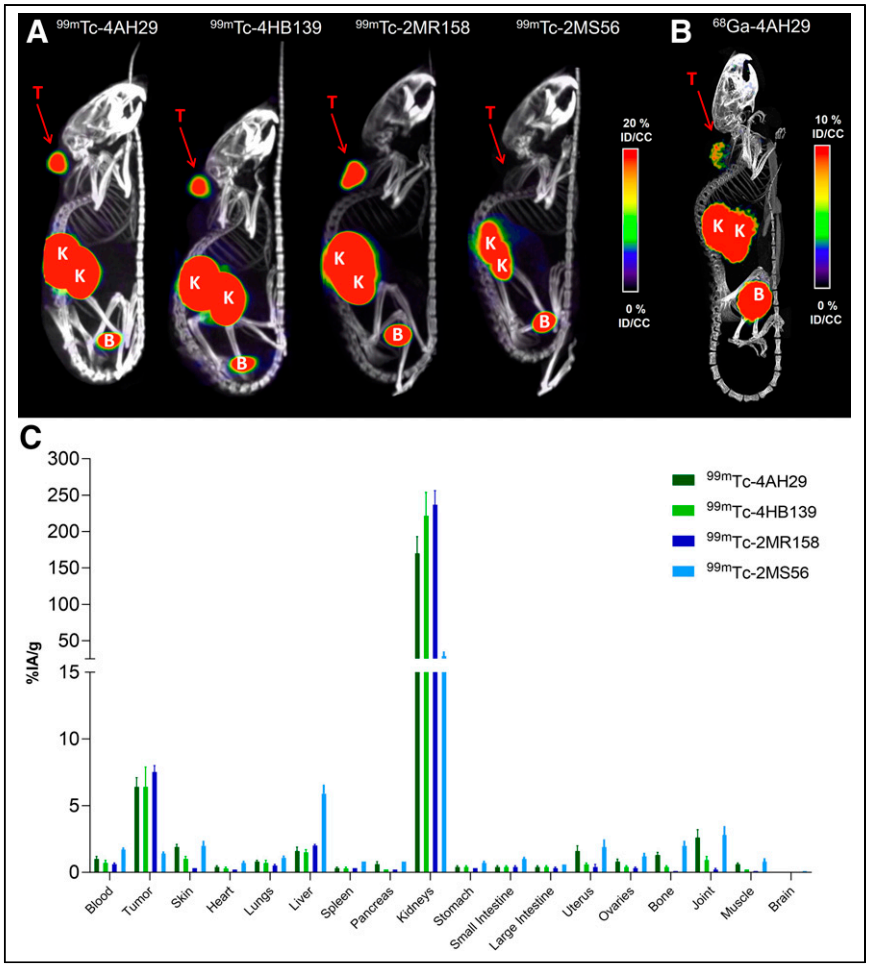

FIGURE 1. Biodistribution of ^{99m}Tc- and ^{68}Ga-labeled anti-FAP sdAbs. (A) Maximum intensity projections (MIPs) corresponding to small-animal SPECT/CT images obtained 1 h after administration of ^{99m}Tc-labeled sdAbs in hFAP-positive U87-MG tumor–xenografted mice (n = 3). (B) MIPs corresponding to small-animal PET/CT image 1 h after administration of [^{68}Ga]Ga-DOTA-4AH29 in hFAP-positive U87-MG tumor–xenografted mice (n = 3). %ID/CC = percentage injected activity per cubic centimeter; B = bladder; K = kidney; T = tumor. (C) Ex vivo biodistribution obtained after dissections 1.5 h after administration of ^{99m}Tc-labeled sdAbs.

increased from 0.34 ± 0.06 at 1 h to 0.52 ± 0.10 at 72 h (Fig. 2C). Slightly elevated uptake was noted in bone, joints, and the uterus (Figs. 2B and 2C). [^{131}I]I-GMIB-4AH29 provided the highest tumor-absorbed dose (0.66 Gy/MBq), with the kidneys receiving 0.23 Gy/MBq, yielding a therapeutic index of 2.9 (Supplemental Table 5). [^{225}Ac]Ac-DOTA-4AH29 delivered 11.45 Gy/0.1 MBq to the kidneys and 7.84 Gy/0.1 MBq to the tumor, resulting in a therapeutic index of 0.7 (Supplemental Table 6). Absorbed doses in other organs and tissues were minimal.

Toxicity Assessment

Mice injected with [^{131}I]I-GMIB-4AH29 completed the 180-d study without weight loss (Figs. 3A and 3B; Supplemental Fig. 9A). Kidney histopathology showed mild to moderate changes at cumulative doses of 167 and 222 MBq (Supplemental Table 7). Conversely, [^{225}Ac]Ac-DOTA-4AH29–treated mice exhibited late-stage toxicity with weight loss (Supplemental Fig. 9B) and reduced survival (129, 138, and 150 d for cumulative doses of 240, 120, and 60 kBq, respectively; Fig. 3C). Dose-dependent kidney histopathologic changes, including tubular damage, fibrosis, and inflammation, began at a cumulative dose of 30 kBq (Supplemental Table 7).

Therapeutic Efficacy

The therapeutic potential of [^{131}I]I-GMIB-4AH29 and [^{225}Ac]Ac-DOTA-4AH29 was evaluated in U87-MG–bearing mice (Fig. 4A). Tumor growth was delayed in all mice receiving α- or β-TRT (Fig. 4B; Supplemental Figs. 10A and 11). No relevant weight loss was observed in the treatment groups (Supplemental Fig. 10B). Consequently, treated mice lived longer than those in the control group ($P < 0.05$; Fig. 4C). No difference in survival was observed between cohorts receiving a high and those receiving a low cumulative radioactive dose of [^{131}I]I-GMIB-4AH29, with mean survival of 52 and 56 d, respectively. One animal of the high-dose group was tumor-free. Median survival was 63 d for a high-dose treatment with [^{225}Ac]Ac-DOTA-4AH29 and 42 d for a low-dose treatment ($P = 0.0001$).

DISCUSSION

FAP is highly expressed on cancer-associated fibroblasts of carcinomas. Breast, colon, and pancreatic tumors often show strong desmoplastic reactions, which result in a dominant presence of stromal cells. FAP has low expression or is undetectable in most normal adult tissues (*8*). Various FAPIs have been used as tools to image FAP expression. Some have also been labeled with therapeutic radionuclides, and although significant efforts were made to optimize the tumor half-life of FAPI compounds, it seems that limited tumor retention still poses a challenge (*9*).

In this study, we identified the lead FAP-targeting sdAb, 4AH29, which has subnanomolar affinity for an mFAP or hFAP conserved epitope and recognizes both purified and membrane-anchored FAP protein. Other relevant FAP-targeting moieties, such as FAPI-04 (*16*), FAPI-46 (*17*), and FAP-2286 (*18*), have been extensively described and underline the relevance of FAP as a promising diagnostic imaging modality. The herein described sdAb 4AH29 is different from the reported FAPIs, because it targets FAP away from the catalytic site. This characteristic is important because FAP enzymatic activity is believed to be involved in normal physiologic processes (*19*). By targeting FAP without affecting its enzymatic activity, this sdAb-based radiopharmaceutical offers a promising avenue for therapeutic interventions without interfering with inherent biologic processes. Moreover, we report here a binding affinity of 38 pM for FAP compared with a nanomolar affinity for most FAPIs, as reported in the literature. We have shown successful specific detection of FAP-positive tumors in mice using [^{68}Ga]Ga-DOTA-4AH29 and tracer-dose [^{131}I]I-GMIB-4AH29. Higher and specific accumulation in FAP-positive tumors was measured, and retention in other tissues was lower than in

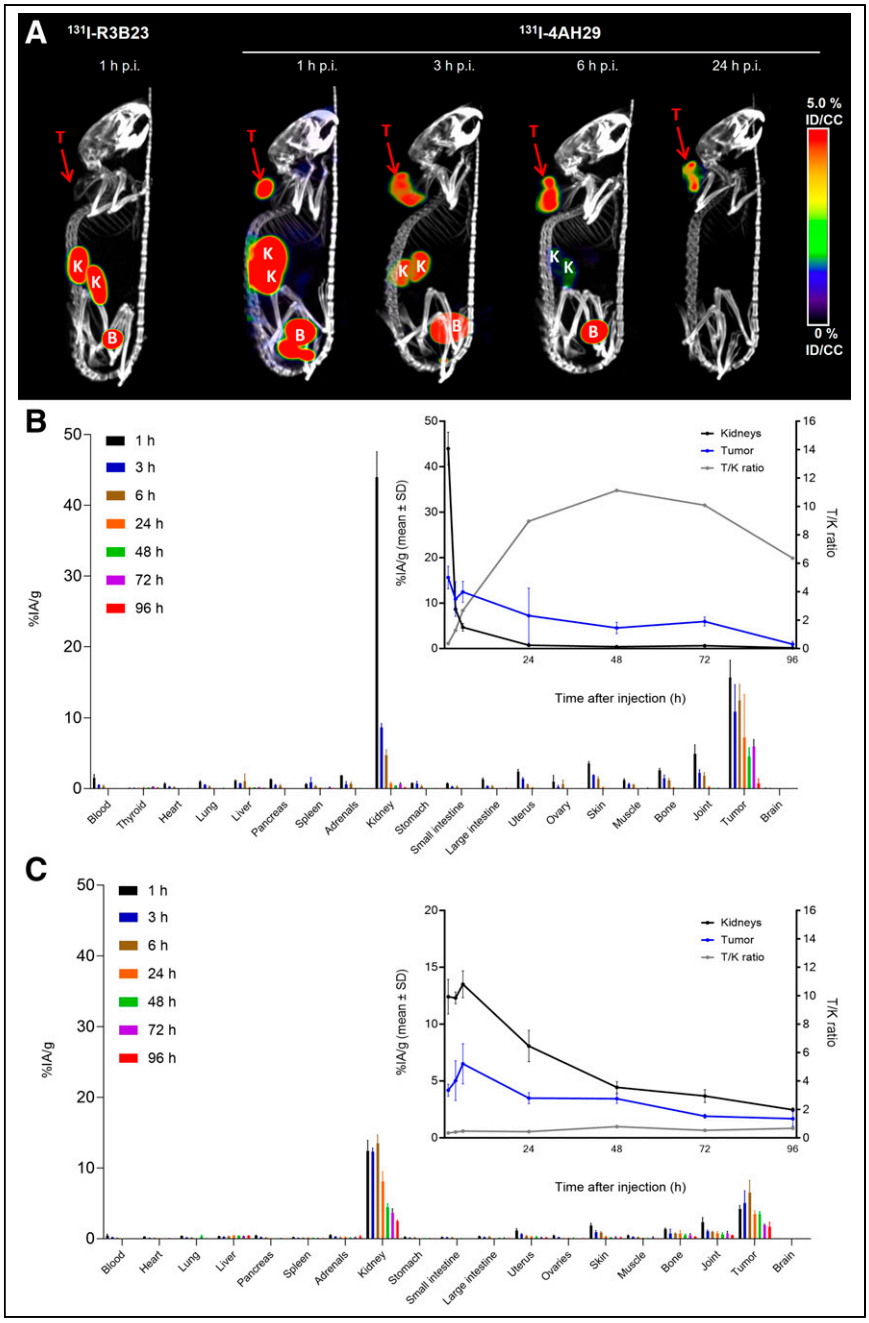

FIGURE 2. Long-term biodistribution of [^{131}I]I-GMIB-4AH29 and [^{225}Ac]Ac-DOTA-4AH29 in hFAP-positive U87-MG tumor–xenografted mice. (A) Maximum intensity projections corresponding to small-animal SPECT/CT images after administration of [^{131}I]I-GMIB-R3B23 and [^{131}I]I-GMIB-4AH29 (n = 3). (B and C) Time-dependent biodistribution after injection of [^{131}I]I-GMIB-4AH29 (n = 3) (B) or [^{225}Ac]Ac-DOTA-4AH29 (n = 3) (C), including tumor-to-kidney ratios. %ID/CC = percentage injected activity per cubic centimeter; B = bladder; K = kidney; p.i. = postinjection; T = tumor.

radiolabeled control sdAb. In the case of tracer-dose [^{131}I]I-GMIB-4AH29, repeated small-animal SPECT/CT underlined its optimal binding characteristics, with radioactivity cleared quickly from circulation and kidneys, whereas retention in the FAP-positive tumor was maintained. This result is in line with what has been reported previously for other ^{131}I-labeled sdAbs, such as the HER2-targeting sdAb 2Rs15d (*14*). Likewise, small-animal PET/CT imaging with [^{68}Ga]Ga-DOTA-4AH29 showed fast (after 1 h) and high-contrast imaging of FAP-positive tumors. The obtained results are in line with what has been described previously for ^{68}Ga-labeled sdAbs such as HER2-targeting 2Rs15d (*20*) and a CD206-targeting sdAb (*21*), both of which are in clinical evaluation (NCT03331601 and NCT03924466, respectively).

For therapeutic purposes, we selected β-emitting ^{131}I and α-emitting ^{225}Ac. The radiohalogen ^{131}I was chosen for the excellent biodistribution that is obtained for sdAbs when radiolabeled with ^{131}I using the prosthetic group SGMIB (*14*). The radiometal ^{225}Ac was chosen for different factors, such as better availability and more straightforward chemistry than with the use of ^{211}At. In theory, the latter is more suited to comparison with ^{131}I. Similar to ^{131}I, the half-life of ^{225}Ac allows centralized manufacturing. However, when used in tandem with fast-clearing moieties, extensive kidney accumulation is an important risk (*13*). Systemic administration of [^{131}I]I-GMIB-4AH29 revealed high and sustained tumor accumulation in hFAP-positive U87-MG–xenografted mice. In this study, we observed varying absolute tumor targeting among different experiments and compounds. For instance, absolute tumor uptake after 1 h measured about 15 %IA/g in the long-term biodistribution of [^{131}I]I-GMIB-4AH29 (Supplemental Table 5), whereas the ex vivo dissections after small-animal SPECT/CT imaging of the same compound revealed tumor uptake of approximately 5 %IA/g (Supplemental Table 3). We and others have observed that the level of FAP expression is dynamic in this naturally FAP-expressing U87-MG cell line because of the variable influence of tumor microenvironmental factors (*22,23*). Hence, comparison of uptake values between different experiments should be done with care. In this study, we assessed the time-dependent biodistribution of [^{131}I]I-GMIB-4AH29 and [^{225}Ac]Ac-DOTA-4AH29 head to head, because only this allows a true comparison. Both drug products accumulated rapidly and specifically in tumors. Unbound [^{131}I]I-GMIB-4AH29 was rapidly cleared from kidneys, with less than 1 %IA/g after 24 h, whereas it was slower for [^{225}Ac]Ac-DOTA-4AH29, with roughly 10 %IA/g still in the kidneys after 24 h. This difference in kidney clearance was expected and has been described previously (*13,14*).

Subsequent assessment of long-term toxicity after repeated administration of therapeutic [^{131}I]I-GMIB-4AH29 and [^{225}Ac]Ac-DOTA-4AH29 further underbuilt this observation. Under the conditions of this preclinical study, intravenous administration of [^{225}Ac]Ac-DOTA-4AH29 to naïve mice twice a week

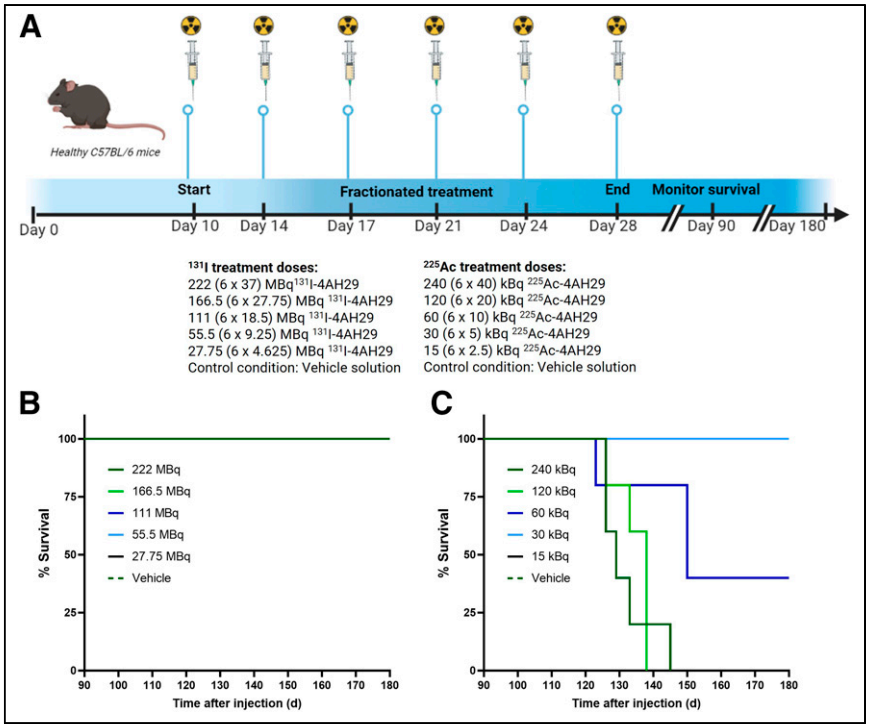

FIGURE 3. Toxicity assessment of therapeutic [^{131}I]I-GMIB-4AH29 and [^{225}Ac]Ac-DOTA-4AH29. (A) C57BL/6 mice were injected with different doses of [^{131}I]I-GMIB-4AH29 or [^{225}Ac]Ac-DOTA-4AH29 (n = 5). (B and C) Kaplan–Meier survival curves were obtained after administration of [^{131}I]I-GMIB-4AH29 (B) or [^{225}Ac]Ac-DOTA-4AH29 (C).

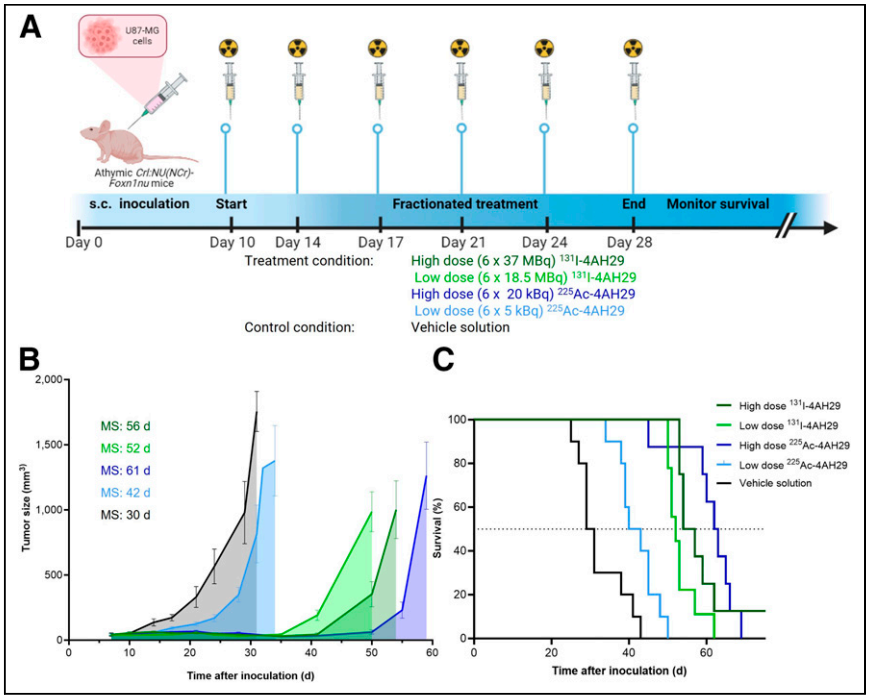

FIGURE 4. Therapeutic efficacy of [^{131}I]I-GMIB-4AH29 and [^{225}Ac]Ac-DOTA-4AH29. (A) Therapeutic potential of [^{131}I]I-GMIB-4AH29 and [^{225}Ac]Ac-DOTA-4AH29 was evaluated in U87-MG tumor–bearing mice (n = 10). (B) Subcutaneous tumor development over time for each treatment group. (C) Kaplan–Meier survival curve obtained after administration of [^{131}I]I-GMIB-4AH29 or [^{225}Ac]Ac-DOTA-4AH29. MS = median survival; s.c. = subcutaneous.

over 3 wk was associated with dose-dependent histopathologic changes in the kidneys after 6 mo. Renal changes were considered adverse and started at cumulative radioactivity doses of 30 kBq. Mice receiving a cumulative dose of 30 kBq did reach the end of the study, after 6 mo, without relevant weight loss. In the case of [^{131}I]I-GMIB-4AH29, mice in all treatment groups lived until the end of the study without the occurrence of weight loss. Histopathologic analysis revealed a limited number of cellular changes in the kidneys for the highest cumulative doses of [^{131}I]I-GMIB-4AH29, whereas the damage was more striking for [^{225}Ac]Ac-DOTA-4AH29. This observation underlines the impact of the radiolabel and linking chemistry on the overall behavior of the radiopharmaceutical.

A few strategies to reduce the retention of cytotoxic radiation in the kidneys after peptide- or small-protein–based TRT have been explored. SdAbs are excreted via the kidneys' glomerulus with moderate retention, making kidneys the dose-limiting organ of sdAb-mediated TRT. A pretargeting approach could circumvent the limitations imposed by kidneys for sdAb-mediated TRT, as was demonstrated successfully for a ^{177}Lu-labeled Affibody molecule (Affibody AB) (*24*). Other possible avenues are modulation of the sdAb protein sequence, cleavable linkers, and coupling methods to avoid a high radiation burden on the kidneys (*25*).

Repeated administration of [^{225}Ac]Ac-DOTA-4AH29 and [^{131}I]I-GMIB-4AH29 in mice bearing hFAP-positive U87-MG xenografts translated into dose-dependent therapeutic effects, with inhibition of tumor development and extended survival for treated mice versus controls. For both radiopharmaceuticals, we aimed to include 1 treatment arm that gave rise to an absorbed dose in the kidneys of roughly 23 Gy, which is the generally accepted threshold for kidney toxicity. However, any reference to this limit should be made with care, because it originates from external-beam irradiation and assumes homogeneous distribution, which is not the case for TRT or for α-particles emitted from ^{225}Ac (*13*). In addition, when considering α-particle radiation, we should consider the relative biological effectiveness to enable comparability of doses from different radiation types. A relative biological effectiveness value of 5 is often used for studies with ^{225}Ac (*26,27*), which always results in higher relative biological effectiveness–weighted absorbed doses in tissues. The second radioactive dose level was selected because of the results from the repeated-dose toxicology in

mice. For [^{131}I]I-GMIB-4AH29, cumulative radioactive doses of 222 and 111 MBq were selected, which correspond to absorbed doses in the kidneys of 50 and 25 Gy, respectively. For [^{225}Ac]Ac-DOTA-4AH29, cumulative radioactive doses of 120 and 30 kBq were selected, leading to kidney-absorbed doses of 14 and 3.5 Gy, respectively. Here, 30 kBq was selected because of the 100% overall survival in the repeated-dose toxicology. These dosimetry estimations assume that the cumulative radioactive dose is delivered in a single administration, which is not the case in this study. A cumulative radioactive dose of 120 kBq was selected to understand the extent of an antitumor effect while considering the likelihood of inducing late-stage toxicity in the kidneys. Because of the short range of α-particles, it remains difficult to determine correctly the maximum tolerable dose and toxicities related to α-particles in small animals, which makes it even more difficult to translate the maximum tolerable dose into patients. Hence, future dose-escalation studies in larger species will be conducted, providing better understanding because the sizeable organs form a more realistic setting to assess the maximum tolerable dose (*28*). High-dose [^{225}Ac]Ac-DOTA-4AH29 performed best, as reflected in the most pronounced tumor inhibition and extended survival, whereas the low-dose treatment gave rise to limited therapeutic signals. This is an important observation, because the low-dose regimen (and beyond) gave rise to adverse renal changes in the repeated-dose toxicology study. Both high- and low-dose [^{131}I]I-GMIB-4AH29 performed well, with relevant impact on both tumor growth inhibition and improved survival of tumor-bearing mice and limited cellular changes in the kidneys, as determined by histopathology.

CONCLUSION

This pioneering study explores the radiotheranostic potential of anti-FAP sdAbs, highlighting sdAb 4AH29's promise in TRT. [^{68}Ga]Ga-DOTA-4AH29 and [^{131}I]I-GMIB-4AH29 enable precise FAP-positive tumor detection. Therapeutic [^{225}Ac]Ac-DOTA-4AH29 and [^{131}I]I-GMIB-4AH29 exhibit potent and sustained tumor targeting, leading to dose-dependent therapeutic effects in FAP-positive tumor-bearing mice. However, further research is necessary to understand adverse events at high therapeutic doses and to align radiation type with treatment indications.

DISCLOSURE

This work is supported by a subsidy from La Région de Bruxelles-Capitale–Innoviris to Precirix. Yana Dekempeneer, Sam Massa, Francis Santens, Laurent Navarro, Marion Berdal, Melissa Lucero, Ana Antunes, and Matthias D'Huyvetter are employees, and Nick Devoogdt and Tony Lahoutte are consultants, of Precirix NV; all hold ownership interest (including patents) in sdAb radiotherapeutics. No other potential conflict of interest relevant to this article was reported.

ACKNOWLEDGMENTS

We thank Claudia Mebis, Marijse Hulsbosch, Jos Eersels, Lina Saadah, Labiba Mahmud, Jonatan Dewulf, and Aleksandra Kotwicka for technical assistance and Peter Covens for assistance with dosimetry.

KEY POINTS

QUESTION: Is radiolabeled sdAb 4AH29 a relevant radiotheranostic tool for FAP-positive cancers?

PERTINENT FINDINGS: SdAb 4AH29 was identified with picomolar affinity for a FAP conserved epitope that is away from the catalytic site and recognized both purified and membrane-anchored FAP protein. [^{68}Ga]Ga-DOTA-4AH29 and tracer-dose [^{131}I]I-GMIB-4AH29 allow specific detection of FAP-positive tumors in mice. Therapeutic [^{225}Ac]Ac-DOTA-4AH29 and [^{131}I]I-GMIB-4AH29 revealed high and sustained tumor targeting, which translated into dose-dependent therapeutic effects in FAP-positive tumor-xenografted mice.

IMPLICATIONS FOR PATIENT CARE: The results presented herein underline the radiotheranostic potential of radiolabeled sdAb 4AH29 for FAP-positive cancers, which warrants clinical testing. SdAbs might benefit patients with breast, colon, and pancreatic tumors, which often show a dominant presence of stromal cells.

REFERENCES

1. Sgouros G, Bodei L, Mcdevitt MR, Nedrow JR. Radiopharmaceutical therapy in cancer: clinical advances and challenges. *Nat Rev Drug Discov.* 2020;19:589–608.
2. D'Huyvetter M, Xavier C, Caveliers V, et al. Radiolabeled nanobodies as theranostic tools in targeted radionuclide therapy of cancer. *Expert Opin Drug Deliv.* 2014;11:1939–1954.
3. Dekempeneer Y, Keyaerts M, Krasniqi A, et al. Targeted alpha therapy using short-lived alpha-particles and the promise of nanobodies as targeting vehicle. *Expert Opin Biol Ther.* 2016;16:1035–1047.
4. Harris PE, Zhernosekov K. The evolution of PRRT for the treatment of neuroendocrine tumors: what comes next? *Front Endocrinol (Lausanne).* 2022;13:941832.
5. Fallah J, Agrawal S, Gittleman H, Fiero MH, Subramaniam S, John C. FDA approval summary: lutetium Lu 177 vipivotide tetraxetan for patients with metastatic castration-resistant prostate cancer. *Clin Cancer Res.* 2023;29:1651–1657.
6. Awad RM, Meeus F, Ceuppens H, et al. Emerging applications of nanobodies in cancer therapy. *Int Rev Cell Mol Biol.* 2022;369:143–199.
7. Wei W, Younis MH, Lan X, Liu J, Cai W. Single-domain antibody theranostics on the horizon. *J Nucl Med.* 2022;63:1475–1479.
8. Puré E, Blomberg R. Pro-tumorigenic roles of fibroblast activation protein in cancer: back to the basics. *Oncogene.* 2018;37:4343–4357.
9. Zhao L, Chen J, Pang Y, et al. Fibroblast activation protein-based theranostics in cancer research: a state-of-the-art review. *Theranostics.* 2022;12:1557–1569.
10. Broisat A, Hernot S, Toczek J, et al. Nanobodies targeting mouse/human VCAM1 for the nuclear imaging of atherosclerotic lesions. *Circ Res.* 2012;110:927–937.
11. Baldi L, Muller N, Picasso S, et al. Transient gene expression in suspension HEK-293 cells: application to large-scale protein production. *Biotechnol Prog.* 2005;21:148–153.
12. Vaneycken I, Devoogdt N, Van Gassen N, et al. Preclinical screening of anti-HER2 nanobodies for molecular imaging of breast cancer. *FASEB J.* 2011;25:2433–2446.
13. Rodak M, Dekempeneer Y, Caveliers V, et al. Preclinical evaluation of ^{225}Ac-labeled single domain antibody for the treatment of HER2pos cancer. *Mol Cancer Ther.* 2022;21:1835–1845.
14. D'Huyvetter M, De Vos J, Xavier C, et al. ^{131}I-labeled anti-HER2 camelid sdAb as a theranostic tool in cancer treatment. *Clin Cancer Res.* 2017;23:6616–6628.
15. Keane FM, Yao TW, Seelk S, et al. Quantitation of fibroblast activation protein (FAP)–specific protease activity in mouse, baboon and human fluids and organs. *FEBS Open Bio.* 2013;4:43–54.
16. Lindner T, Loktev A, Altmann A, et al. Development of quinoline-based theranostic ligands for the targeting of fibroblast activation protein. *J Nucl Med.* 2018;59:1415–1422.
17. Loktev A, Lindner T, Burger E, et al. Development of fibroblast activation protein–targeted radiotracers with improved tumor retention. *J Nucl Med.* 2019;60:1421–1429.

18. Zboralski D, Hoehne A, Bredenbeck A, et al. Preclinical evaluation of FAP-2286 for fibroblast activation protein targeted radionuclide imaging and therapy. *Eur J Nucl Med Mol Imaging.* 2022;49:3651–3667.
19. Juillerat-Jeanneret L, Tafelmeyer P, Golshayan D. Fibroblast activation protein-α in fibrogenic disorders and cancer: more than a prolyl-specific peptidase? *Expert Opin Ther Targets.* 2017;21:977–991.
20. Xavier C, Vaneycken I, D'Huyvetter M, et al. Synthesis, preclinical validation, dosimetry, and toxicity of ^{68}Ga-NOTA-anti-HER2 nanobodies for iPET imaging of HER2 receptor expression in cancer. *J Nucl Med.* 2013;54:776–784.
21. Xavier C, Blykers A, Laoui D, et al. Clinical translation of [^{68}Ga]Ga-NOTA-anti-MMR-sdAb for PET/CT imaging of protumorigenic macrophages. *Mol Imaging Biol.* 2019;21:898–906.
22. Krepela E, Vanickova Z, Hrabal P, et al. Regulation of fibroblast activation protein by transforming growth factor beta-1 in glioblastoma microenvironment. *Int J Mol Sci.* 2021;22:1046.
23. Röhrich M, Loktev A, Wefers AK, et al. IDH-wildtype glioblastomas and grade III/IV IDH-mutant gliomas show elevated tracer uptake in fibroblast activation protein–specific PET/CT. *Eur J Nucl Med Mol Imaging.* 2019;46:2569–2580.
24. Westerlund K, Altai M, Mitran B, et al. Radionuclide therapy of HER2-expressing human xenografts using Affibody-based peptide nucleic acid-mediated pretargeting: in vivo proof of principle. *J Nucl Med.* 2018;59:1092–1098.
25. Chigoho DM, Bridoux J, Hernot S. Reducing the renal retention of low- to moderate-molecular-weight radiopharmaceuticals. *Curr Opin Chem Biol.* 2021;63:219–228.
26. Kratochwil C, Bruchertseifer F, Giesel F, Apostolidis C, Haberkorn U, Morgenstern A. Ac-225-DOTATOC: an empiric dose finding for alpha particle emitter based radionuclide therapy of neuroendocrine tumors [abstract]. *J Nucl Med.* 2015;56(suppl 3):S1232.
27. Kratochwil C, Bruchertseifer F, Rathke H, et al. Targeted α-therapy of metastatic castration-resistant prostate cancer with ^{225}Ac-PSMA-617: dosimetry estimate and empiric dose finding. *J Nucl Med.* 2017;58:1624–1631.
28. Castillo Seoane D, de Saint-Hubert M, Crabbe M, Struelens L, Koole M. Targeted alpha therapy: a critical review of translational dosimetry research with emphasis on actinium-225. *Q J Nucl Med Mol Imaging.* 2020;64:265–277.